

Spin-Peierls Transition in ZnCr_2O_4 and MgCr_2O_4 – Supplemental Material –

Ludovic D. C. Jaubert,^{1,2} Yasir Iqbal,² and Harald O. Jeschke^{3,2}

¹CNRS, University of Bordeaux, LOMA, UMR 5798, F-33400 Talence, France

²Department of Physics and Quantum Centre of Excellence for Diamond and Emergent Materials (QuCenDiEM),
Indian Institute of Technology Madras, Chennai 600036, India

³Research Institute for Interdisciplinary Science, Okayama University, Okayama 700-8530, Japan

I. DFT ENERGY MAPPING METHOD AND ADDITIONAL RESULTS

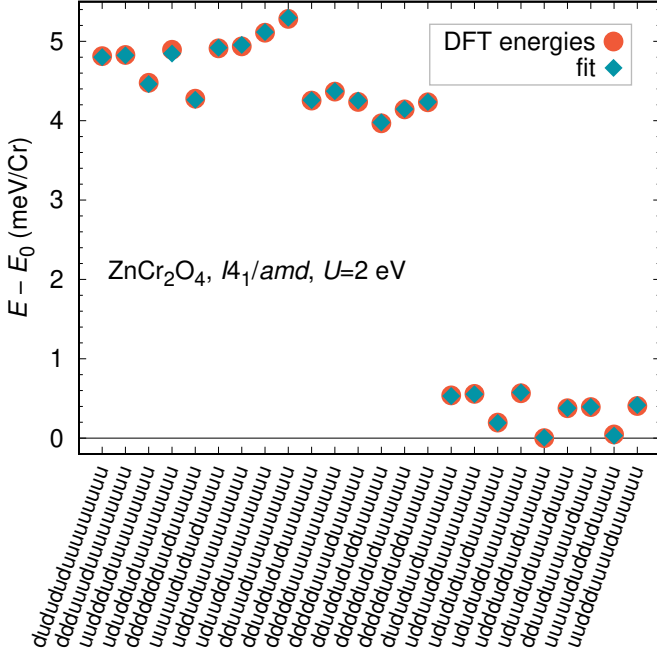


FIG. 1. Calculated total energies for the tetragonal $I4_1/amd$ structure of ZnCr_2O_4 at $U = 2\text{eV}$, compared to the energies of the Heisenberg Hamiltonian. The fit is almost perfect.

The density functional theory (DFT) energy mapping method requires the calculation of a large number of magnetic energies for spin configurations; these are then mapped to the Heisenberg Hamiltonian to extract the exchange interactions. For this purpose, we perform DFT calculations with the all electron full potential local orbital (FPLO) basis [1] and the generalized gradient approximation to the exchange correlation functional [2]. We apply the DFT+U method [3] to the strongly correlated $3d$ orbitals of the Cr^{3+} ions. We fixed the Hund's rule coupling J_H to a literature value $J_H = 0.72\text{eV}$ [4] and only varied the on-site interaction strength U . An important aspect to the approach is that we use many more energies than would be required to solve for the exchange interactions and find the optimal solution using singular value decomposition. In this way, we get statistical information on the error bars of the exchange couplings, and a randomly incorrect energy cannot derail

the entire calculation. As an example for the procedure, Fig. 1 shows the comparison between DFT and Heisenberg Hamiltonian energies for one example (the $U = 2\text{eV}$ line in Table VI). The almost perfect fit indicates that the extracted nine exchange interactions reproduce the 24 DFT energies very well. All structures used in this work are given in Table I.

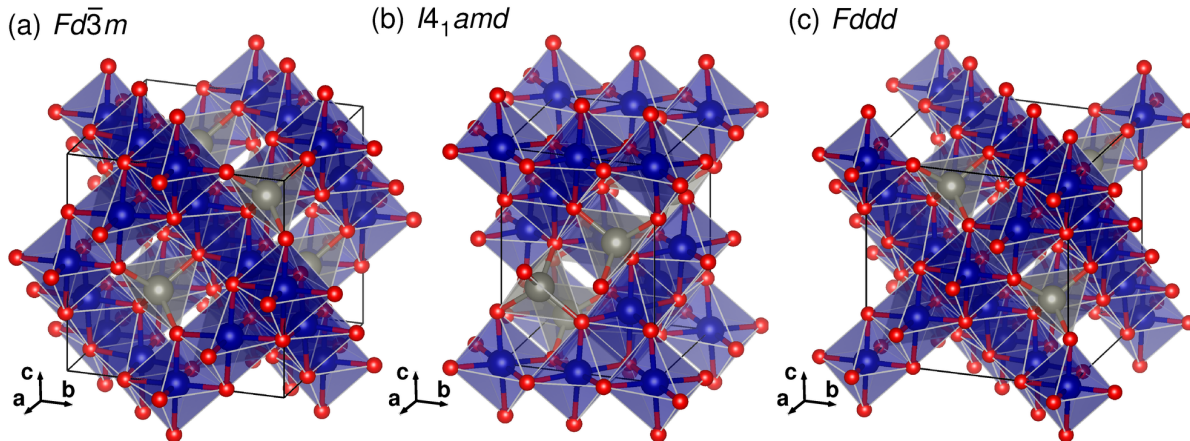
In Tables II-IX, we present the full results of the DFT energy mapping calculations. Bold lines are interpolated to yield the experimental Curie-Weiss temperatures as explained in the main text. Bonds are partly identified by bond lengths which are given in the last line of the tables. We converged the energies of the $2 \times 1 \times 1$ supercells of the cubic structures with $8 \times 8 \times 8$ k meshes and the energies of the $2 \times 2 \times 1$ supercells of the tetragonal and orthorhombic structures with $6 \times 6 \times 6$ k meshes.

II. MORE DETAILS ABOUT THE CUBIC MgCr_2O_4 HAMILTONIAN

For cubic MgCr_2O_4 , our Hamiltonian (given as bold line in Table III) differs slightly from the Hamiltonian extracted from inelastic neutron scattering by Bai *et al.* [9]. Therefore, we investigated if the DFT energy mapping result has a significant dependence on the crystal structure we use for the calculation. Low temperature cubic structures for MgCr_2O_4 have been determined by Dutton *et al.* [5], Ortega-San-Martín *et al.* [7] and by Gao *et al.* [8]. The full results for the DFT energy mapping for these structures is contained in Tables III, IV and V, respectively. All three calculations agree in the crucial details: the most important subleading coupling is antiferromagnetic $J_{3a} \sim 2\text{K}$, followed by antiferromagnetic $J_{3b} \sim 0.5\text{K}$ and ferromagnetic $J_2 \sim -0.4\text{K}$. Thus, the result of the DFT energy mapping is solid and the small disagreement with the INS fit is probably not due to uncertainties in the structure determination. In fact, we also confirmed for the Gao *et al.* [8] structure that DFT relaxation of the oxygen coordinate does not change this conclusion. Neither does resolution of more exchange interactions: For the Gao *et al.* [8] structure, we determined also J_4 (and J_6). At $J_4 = -0.07\text{K}$, it is almost impossible to resolve and not resolving it definitely does not add significant error to any of the other couplings.

TABLE I. Structures used in this work.

material	space group	T_{exp} (K)	a (Å)	b (Å)	c (Å)	Zn/Mg	Cr	O	reference
ZnCr ₂ O ₄	$Fd\bar{3}m$	15	8.31948	–	–	8a	16d	32e (0.2622 0.2622 0.2622)	[5]
ZnCr ₂ O ₄	$I4_1/amd$	5.4	5.8875	–	8.3090	4b	8d	16h (0.000 0.52500 0.73790)	[6]
ZnCr ₂ O ₄	$Fddd$	5.7	8.343	8.3012	8.3144	8a	16d	32h (0.01193 0.23534 0.00722)	[6]
MgCr ₂ O ₄	$Fd\bar{3}m$	15	8.32768	–	–	8a	16d	32e (0.2591 0.2591 0.2591)	[5]
MgCr ₂ O ₄	$Fd\bar{3}m$	19	8.3329	–	–	8a	16d	32e (0.2612 0.2612 0.2612)	[7]
MgCr ₂ O ₄	$Fd\bar{3}m$	20	8.3196	–	–	8a	16d	32e (0.261 0.261 0.261)	[8]
MgCr ₂ O ₄	$I4_1/amd$	10	5.8961	–	8.3211	4b	8d	16h (0.000 0.5224 0.7393)	[7]
MgCr ₂ O ₄	$Fddd$	5.4	8.3041	8.3228	8.3526	8a	16d	32h (0.01130 0.23865 0.01093)	[6]

FIG. 2. Structures of ZnCr₂O₄. The coordinates are given in Table I.TABLE II. Exchange couplings of cubic ZnCr₂O₄, calculated within GGA+U. The structure from Ref. [5] determined at $T = 15$ K was used.

U (eV)	J_1 (K)	J_2 (K)	J_{3a} (K)	J_{3b} (K)	T_{CW} (K)
1.25	62.0(4)	0.4(2)	2.5(3)	2.4(3)	-508.5
1.5	56.0(3)	0.3(2)	2.3(3)	2.3(3)	-458.7
1.75	50.6(3)	0.2(2)	2.0(2)	2.1(2)	-414.2
1.90	47.6(3)	0.2(2)	1.9(2)	2.0(2)	-390
2.	45.7(2)	0.2(2)	1.9(2)	2.0(2)	-374.3
2.25	41.3(2)	0.1(1)	1.7(2)	1.8(2)	-338.4
2.5	37.3(2)	0.1(1)	1.6(1)	1.7(1)	-305.8
$d_{\text{Cr-Cr}}$ (Å)	2.94138	5.09462	5.88276	5.88276	

III. ELECTRONIC ENERGIES

For corroborating the spin-Peierls scenario we outline in the main text, it would be best to consider the entire energy balance to clearly see the place of the magnetic energy gain in the spin-Peierls transition. However, the electronic energy alone calculated from the experimental crystal structures is insufficient for this purpose. A future, more comprehensive study would involve ab-initio molecular dynamics which would have two essential features: (i) it would permit equilibration of the structures at a given temperature near the transition, taking out inevitable potential energy contributions that are due to the fact that even a very precise experimental crystal structure of ZnCr₂O₄ or MgCr₂O₄ at, say, $T = 10$ K, will

TABLE III. Exchange couplings of cubic MgCr₂O₄, calculated within GGA+U. The structure from Ref. [5] determined at $T = 15$ K was used.

U (eV)	J_1 (K)	J_2 (K)	J_{3a} (K)	J_{3b} (K)	T_{CW} (K)
1.25	78.7(4)	-0.4(3)	2.5(3)	0.7(3)	-608.9
1.5	72.0(3)	-0.4(2)	2.3(2)	0.7(3)	-556.6
1.75	66.0(3)	-0.4(2)	2.1(2)	0.6(2)	-509.7
2.	60.6(2)	-0.4(2)	1.9(2)	0.6(2)	-467.5
2.25	55.7(2)	-0.4(1)	1.7(2)	0.6(2)	-429.3
2.46	51.9(2)	-0.4(1)	1.6(2)	0.5(2)	-400
2.5	51.2(2)	-0.4(1)	1.6(1)	0.5(1)	-394.6
$d_{\text{Cr-Cr}}$ (Å)	2.94428	5.09964	5.88856	5.88856	

be, due to error bars on lattice parameters and oxygen position, a small distance in parameter space and therefore a non-negligible distance in energy from the DFT optimum. (ii) This approach would also introduce the small vibrational energy that is part of the energy balance at ~ 14 K. As a rough approximation to this, we determine an approximate electronic energy that is relevant to the transition. We use DFT to relax the only free internal position in the three crystal structures, the oxygen position. We do this because experimentally, determining the oxygen position precisely is difficult, in particular using x-ray diffraction, so this position is likely to carry some error. Note that full structural relaxation would not be helpful here because for the $T \sim 14$ K phase transition, the zero temperature lattice parameter and lat-

TABLE IV. Exchange couplings of cubic MgCr_2O_4 , calculated within GGA+U. The structure from Ref. [7] determined at $T = 19\text{ K}$ by neutron diffraction was used.

U (eV)	J_1 (K)	J_2 (K)	J_{3a} (K)	J_{3b} (K)	T_{CW} (K)
1.5	61.6(3)	-0.2(2)	2.5(3)	0.7(3)	-482.7
1.75	56.1(3)	-0.2(2)	2.2(2)	0.7(3)	-438.7
1.994	51.2(2)	-0.3(2)	2.0(2)	0.6(3)	400
2.	51.1(2)	-0.3(2)	2.0(2)	0.6(2)	-399.1
2.25	46.5(2)	-0.3(1)	1.9(2)	0.6(2)	-363.5
2.5	42.4(2)	-0.3(1)	1.7(2)	0.5(2)	-331.1
2.75	38.7(2)	-0.3(1)	1.6(1)	0.5(2)	-301.7
<hr/>					
$d_{\text{Cr-Cr}}$ (Å)	2.94613	5.10284	5.89225	5.89225	

TABLE V. Exchange couplings of cubic MgCr_2O_4 , calculated within GGA+U. The structure from Ref. [8] determined at $T = 20\text{ K}$ by powder synchrotron X-ray diffraction was used.

U (eV)	J_1 (K)	J_2 (K)	J_{3a} (K)	J_{3b} (K)	T_{CW} (K)
1.5	63.9(3)	-0.2(2)	2.5(3)	0.8(3)	-500.6
1.75	58.2(3)	-0.2(2)	2.3(2)	0.7(3)	-455.3
2.	53.1(2)	-0.3(2)	2.1(2)	0.7(2)	-414.7
2.097	51.2(2)	-0.3(2)	2.0(2)	0.6(2)	400
2.25	48.4(2)	-0.3(2)	1.9(2)	0.6(2)	-378.1
2.5	44.2(2)	-0.3(1)	1.7(2)	0.6(2)	-344.8
2.75	40.4(2)	-0.3(1)	1.6(1)	0.5(2)	-314.5
<hr/>					
$d_{\text{Cr-Cr}}$ (Å)	2.94142	5.09469	5.88285	5.88285	

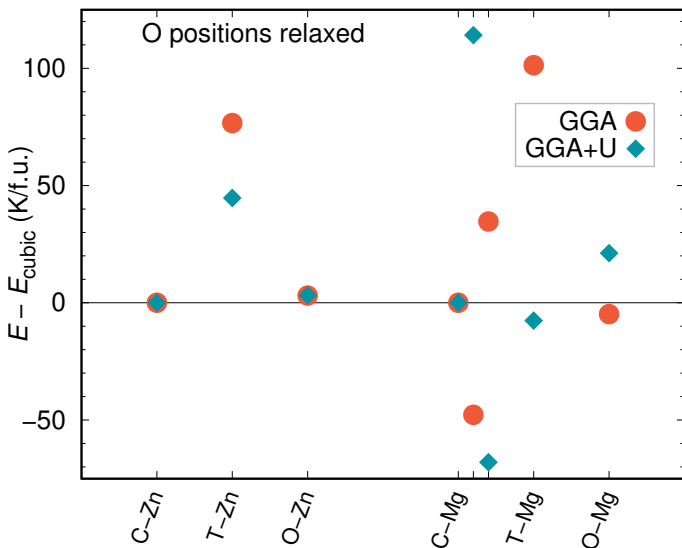


FIG. 3. Comparison of electronic energies of ZnCr_2O_4 or MgCr_2O_4 obtained by optimizing the oxygen positions using nonmagnetic GGA and spin-polarized GGA+U calculations. Abbreviations C-Zn, T-Zn and O-Zn are for cubic ZnCr_2O_4 , tetragonal ZnCr_2O_4 and orthorhombic ZnCr_2O_4 structures, and the same holds for MgCr_2O_4 . At the C-Mg label, energies for three cubic MgCr_2O_4 structures are given in the order Dutton *et al.* [5], Ortega-San-Martín *et al.* [7] and Gao *et al.* [8].

tice symmetry are not relevant. Fig. 3 shows the two sets of energies, determined with nonmagnetic GGA and spin-polarized GGA+U calculations, respectively. As the

GGA+U, $U = 2\text{ eV}$ functional describes the magnetic Hamiltonian correctly, we consider this to be the better approximation. The figure demonstrates that electronically, the structures with different symmetry can be extremely close, as for example the ZnCr_2O_4 cubic and orthorhombic structures or the MgCr_2O_4 cubic and tetragonal structures, both calculated within GGA+U. This means that the magnetic energy jump of $\sim 15\text{ K}$ per formula unit (note that Figs. 2(c,d) of the main text give energies per spin) is very relevant in comparison which supports our spin-Peierls scenario. However, we can also see that some other electronic energy comparisons are not that close even if energy scales are still comparable. It is these cases where the more comprehensive approach outlined above of finite temperature ab-initio molecular dynamics would be needed for a definite answer because it would allow reconciliation between lattice parameters determined near the transition temperature and DFT optima at the same temperature. To show that experimental crystal structures with the same symmetry taken at very similar temperatures can yield substantially different electronic energies, we have included in Fig. 3 electronic energies for the three cubic MgCr_2O_4 structures we considered. The fact that their energies can vary by as much as 100 K shows that the present approach is incomplete and needs further investigation which is beyond the scope of the present study.

IV. DETAILS OF MONTE CARLO SIMULATIONS

Monte Carlo simulations are performed on systems of classical Heisenberg spins with $N = 16L^3$ sites, where L^3 is the number of cubic unit cells. The spin length is $\sqrt{S(S+1)} = \sqrt{15}/2$. Several update algorithms are used together: the heatbath method, over-relaxation and parallel tempering. Parallel tempering is done every 100 Monte Carlo steps (MCs) and overrelaxation is done at every MCs. Thermalization is made in two steps: first a slow annealing from high temperature to the temperature of measurement T during t_{eq} MCs followed by t_{eq} MCs at temperature T . After thermalization, measurements are done every 10 MCs during t_m MCs.

The parameters of our simulations are $N = 8192$ spins for $t_m = 2t_{eq} = 10^7$ MCs for thermodynamic quantities in Fig. 3(a,b,c,d), and $N = 128000$ spins for $t_m = 10t_{eq} = 5 \cdot 10^5$ MCs for the structure factor in Fig. 3(e).

The structure factor in Fig. 3(e) has been computed as would be measured by neutron scattering:

$$S(\mathbf{q}) = F(|\mathbf{q}|) \frac{1}{N} \left| \sum_{i=1}^N \mathbf{S}_i^\perp \exp(i\mathbf{q} \cdot \mathbf{r}_i) \right|, \quad (1)$$

where \mathbf{r}_i is the position of site i and \mathbf{S}_i^\perp is the vector spin \mathbf{S}_i projected in the plane orthogonal to the wavevector

TABLE VI. Exchange couplings of tetragonal ZnCr_2O_4 , calculated within GGA+U. The structure from Ref. [6] determined at $T = 5.4\text{ K}$ was used.

U (eV)	J_1^{xy} (K)	J_1^z (K)	J_2 (K)	J_2' (K)	J_{3a}^{xy} (K)	J_{3b}^{xy} (K)	J_{3a}^z (K)	J_{3b}^z (K)	J_7 (K)	T_{CW} (K)
1.25	61.9(3)	60.1(2)	0.5(5)	0.5(2)	2.6(4)	2.2(4)	2.7(5)	2.2(4)	-0.2(2)	-502.2
1.5	55.8(3)	54.2(2)	0.4(4)	0.4(2)	2.3(3)	2.1(3)	2.4(4)	2.1(3)	-0.2(2)	-452.7
1.75	50.4(2)	48.8(2)	0.3(4)	0.3(1)	2.1(3)	2.0(3)	2.1(3)	1.9(3)	-0.2(1)	-408.6
1.86	48.2(2)	46.6(2)	0.3(4)	0.3(1)	2.0(3)	1.9(3)	2.0(3)	1.9(3)	-0.1(1)	-390
2.	45.6(2)	44.1(1)	0.2(3)	0.3(1)	1.9(2)	1.8(2)	1.9(3)	1.8(2)	-0.1(1)	-368.9
2.25	41.2(2)	39.7(1)	0.2(3)	0.2(1)	1.7(2)	1.7(2)	1.7(2)	1.7(2)	-0.1(1)	-333.2
2.5	37.2(2)	35.8(1)	0.1(2)	0.2(1)	1.6(2)	1.6(2)	1.6(2)	1.6(2)	-0.1(1)	-300.9
$d_{\text{Cr-Cr}}(\text{\AA})$	2.94071	2.94375	5.09171	5.09697	5.88143	5.88143	5.8875	5.8875	6.5702	

TABLE VII. Exchange couplings of tetragonal MgCr_2O_4 , calculated within GGA+U. The structure from Ref. [7] determined at $T = 10\text{ K}$ was used.

U (eV)	J_1^{xy} (K)	J_1^z (K)	J_2 (K)	J_2' (K)	J_{3a}^{xy} (K)	J_{3b}^{xy} (K)	J_{3a}^z (K)	J_{3b}^z (K)	J_7 (K)	T_{CW} (K)
1.25	69.4(4)	67.3(3)	-0.1(6)	0.1(2)	2.6(5)	0.4(5)	3.1(5)	0.8(5)	-0.4(2)	-539.1
1.5	63.1(3)	61.1(2)	-0.1(5)	0.0(2)	2.4(4)	0.4(4)	2.8(5)	0.7(4)	-0.3(2)	-489.4
1.75	57.5(3)	55.6(2)	-0.2(4)	0.0(2)	2.2(3)	0.4(3)	2.5(4)	0.7(3)	-0.3(2)	-445.0
2.	52.5(2)	50.6(2)	-0.2(4)	-0.1(1)	2.0(3)	0.4(3)	2.2(3)	0.6(3)	-0.3(1)	-405.2
2.03	51.8(2)	50.0(2)	-0.2(4)	-0.1(1)	2.0(3)	0.4(3)	2.2(3)	0.6(3)	-0.3(1)	-400
2.25	47.9(2)	46.1(2)	-0.2(3)	-0.1(1)	1.8(2)	0.4(2)	2.0(3)	0.6(2)	-0.2(1)	-369.2
2.5	43.7(2)	42.0(1)	-0.2(3)	-0.1(1)	1.7(2)	0.4(2)	1.8(2)	0.5(2)	-0.2(1)	-336.7
$d_{\text{Cr-Cr}}(\text{\AA})$	2.945	2.94805	5.09913	5.10441	5.89001	5.89001	5.8961	5.8961	6.57977	

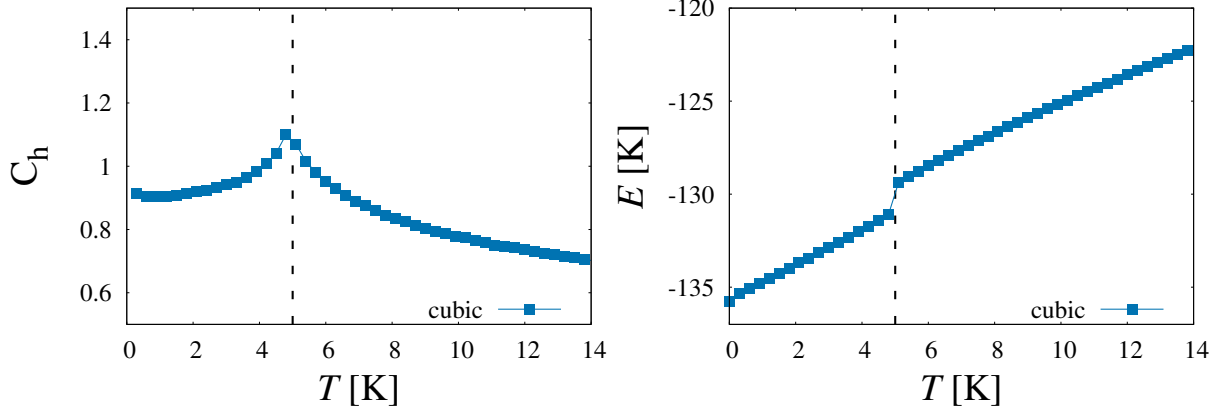


FIG. 4. **Monte Carlo simulations:** Specific heat (left) and energy per spin (right) for parameters of MgCr_2O_4 obtained from Ref. [9] in the cubic regime: $\{J_1, J_2, J_{3a}, J_{3b}\} = \{38.05, 3.10, 4.00, 0.32\}$ K. As expected, the transition temperature found in simulations for the cubic structure (dashed line at 5K) is lower than the experimental value of T_N . Using Bai's parameters [9] does not affect the main conclusions of our paper.

\mathbf{q} , as seen by neutrons. $F(\mathbf{q})$ is the tabulated form factor of Cr(III) ions.

-
- [1] K. Koepnik and H. Eschrig, Full-potential nonorthogonal local-orbital minimum-basis band-structure scheme, *Phys. Rev. B* **59**, 1743 (1999).
- [2] J. P. Perdew, K. Burke, and M. Ernzerhof, Generalized gradient approximation made simple, *Phys. Rev. Lett.* **77**, 3865 (1996).
- [3] A. I. Liechtenstein, V. I. Anisimov, and J. Zaanen, Density-functional theory and strong interactions: Orbital ordering in mott-hubbard insulators, *Phys. Rev. B* **52**, R5467 (1995).
- [4] T. Mizokawa and A. Fujimori, Electronic structure and orbital ordering in perovskite-type 3d transition-metal oxides studied by hartree-fock band-structure calculations, *Phys. Rev. B* **54**, 5368 (1996).
- [5] S. E. Dutton, Q. Huang, O. Tchernyshyov, C. L. Broholm, and R. J. Cava, Sensitivity of the magnetic properties of the ZnCr_2O_4 and MgCr_2O_4 spinels to nonstoichiometry, *Phys. Rev. B* **83**, 064407 (2011).

TABLE VIII. Exchange couplings of orthorhombic ZnCr_2O_4 , calculated within GGA+U. The structure from Ref. [6] determined at $T = 5.7\text{ K}$ was used.

U (eV)	J_1^x (K)	J_1^y (K)	J_1^z (K)	J_2 (K)	J_2' (K)	J_2'' (K)	J_{3a}^x (K)	J_{3b}^x (K)	J_{3a}^z (K)	J_{3b}^z (K)	J_{3a}^y (K)	T_{CW} (K)
1.5	62.8(3)	46.9(2)	73.0(3)	0.2(7)	0.6(2)	-0.4(7)	5.2(3)	4.6(4)	2.8(3)	2.2(3)	-1.0(3)	-493.6
1.75	57.1(2)	42.0(2)	66.7(2)	0.1(6)	0.5(2)	-0.4(6)	4.7(3)	4.3(3)	2.6(3)	2.1(2)	-0.9(3)	-447.6
2.	52.0(2)	37.6(2)	61.0(2)	0.1(5)	0.4(2)	-0.3(5)	4.2(2)	3.9(2)	2.3(2)	1.9(2)	-0.8(2)	-406.3
2.11	49.9(2)	35.9(2)	58.8(2)	0.0(5)	0.4(2)	-0.3(5)	4.1(2)	3.8(2)	2.2(2)	1.9(2)	-0.8(2)	-390
2.25	47.3(2)	33.6(2)	55.9(2)	0.0(4)	0.4(1)	-0.3(4)	3.8(2)	3.7(2)	2.1(2)	1.8(2)	-0.7(2)	-369.1
2.5	43.1(2)	30.0(1)	51.3(1)	0.0(3)	0.3(1)	-0.3(3)	3.5(2)	3.4(2)	2.0(2)	1.7(2)	-0.7(2)	-335.3
$d_{\text{Cr-Cr}}$ (Å)	2.93725	2.94232	2.94464	5.08905	5.09309	5.10185	5.8745	5.8745	5.88463	5.88463	5.88929	

TABLE IX. Exchange couplings of orthorhombic MgCr_2O_4 , calculated within GGA+U. The structure from Ref. [6] determined at $T = 5.4\text{ K}$ was used.

U (eV)	J_1^x (K)	J_1^y (K)	J_1^z (K)	J_2 (K)	J_2' (K)	J_2'' (K)	J_{3a}^x (K)	J_{3b}^x (K)	J_{3a}^z (K)	J_{3b}^z (K)	J_{3a}^y (K)	T_{CW} (K)
1.5	62.0(5)	62.3(5)	62.8(4)	0.8(1.3)	-1.3(1.4)	0.3(5)	3.0(5)	0.7(3)	4.4(7)	1.0(5)	1.1(4)	-491.8
1.75	56.4(4)	56.8(4)	57.1(4)	0.6(1.1)	-1.2(1.1)	0.2(4)	2.6(4)	0.6(2)	3.9(5)	1.0(4)	1.1(4)	-446.7
2.	51.4(3)	51.8(3)	52.0(3)	0.4(9)	-1.0(9)	0.1(3)	2.4(3)	0.6(2)	3.4(5)	1.0(4)	1.0(3)	-406.3
2.04	50.6(2)	51.0(3)	51.2(3)	0.4(9)	-1.0(9)	0.1(3)	2.4(3)	0.6(2)	3.4(5)	0.9(4)	1.0(3)	-400
2.25	46.9(3)	47.3(3)	47.3(3)	0.3(8)	-0.9(8)	0.0(3)	2.2(3)	0.5(2)	3.1(4)	0.9(3)	1.0(3)	-369.9
2.5	42.7(2)	43.2(2)	43.1(2)	0.1(6)	-0.8(7)	0.0(2)	2.0(2)	0.5(2)	2.8(3)	0.9(3)	0.9(2)	-336.9
$d_{\text{Cr-Cr}}$ (Å)	2.93925	2.94453	2.94783	5.09207	5.09779	5.10692	5.8785	5.8785	5.88906	5.88906	5.89565	

- [6] M. C. Kemei, P. T. Barton, S. L. Moffitt, M. W. Gaultois, J. A. Kurzman, R. Seshadri, M. R. Suchomel, and Y.-I. Kim, Crystal structures of spin-Jahn-Teller-ordered MgCr_2O_4 and ZnCr_2O_4 , *J. Phys.: Condens. Matter* **25**, 326001 (2013).
- [7] L. Ortega-San-Martín, A. J. Williams, C. D. Gordon, S. Klemme, and J. P. Attfield, Low temperature neutron diffraction study of MgCr_2O_4 spinel, *J. Phys.: Condens. Matter* **20**, 104238 (2008).
- [8] S. Gao, K. Guratinder, U. Stuhr, J. S. White, M. Mansson, B. Roessli, T. Fennell, V. Tsurkan, A. Loidl, M. Ciomaga Hatnean, G. Balakrishnan, S. Raymond, L. Chapon, V. O. Garlea, A. T. Savici, A. Cervellino, A. Bombardi, D. Chernyshov, C. Rüegg, J. T. Haraldsen, and O. Zaharko, Manifolds of magnetic ordered states and excitations in the almost Heisenberg pyrochlore antiferromagnet MgCr_2O_4 , *Phys. Rev. B* **97**, 134430 (2018).
- [9] X. Bai, J. A. M. Paddison, E. Kapit, S. M. Koohpayeh, J.-J. Wen, S. E. Dutton, A. T. Savici, A. I. Kolesnikov, G. E. Granroth, C. L. Broholm, J. T. Chalker, and M. Mourigal, Magnetic excitations of the classical spin liquid MgCr_2O_4 , *Phys. Rev. Lett.* **122**, 097201 (2019).